

Changes in Real Time: Online Scene Change Detection with Multi-View Fusion

Chamuditha Jayanga Galappaththige^{1,2} Jason Lai³ Lloyd Windrim^{2,4}

Donald Dansereau^{2,3} Niko Sünderhauf^{1,2} Dimity Miller^{1,2}

¹QUT Centre for Robotics ²ARIAM ³ACFR, University of Sydney ⁴Abyss Solutions

{chamuditha.galappaththige, d24.miller}@.qut.edu.au

Abstract

Online Scene Change Detection (SCD) is an extremely challenging problem that requires an agent to detect relevant changes on the fly while observing the scene from unconstrained viewpoints. Existing online SCD methods are significantly less accurate than offline approaches. We present the first online SCD approach that is pose-agnostic, label-free, and ensures multi-view consistency, while operating at over 10 FPS and achieving new state-of-the-art performance, surpassing even the best offline approaches. Our method introduces a new self-supervised fusion loss to infer scene changes from multiple cues and observations, PnP-based fast pose estimation against the reference scene, and a fast change-guided update strategy for the 3D Gaussian Splatting scene representation. Extensive experiments on complex real-world datasets demonstrate that our approach outperforms both online and offline baselines. Code is available at <https://chumsy0725.github.io/O-SCD/>.

1. Introduction

Detecting changes in a scene is an essential task in scene understanding, with numerous applications in environmental monitoring [46], infrastructure inspection [14], and damage assessment [40]. Scene change detection (SCD) is especially challenging in the context of robotics, where an agent observes the scene from unconstrained and independent viewpoints when re-visiting it after some time, while having to discern relevant (e.g. object movement) and irrelevant changes (e.g. caused by shadows, or reflections).

To address these challenges, recent approaches [13, 17, 22, 30, 52] leverage photorealistic 3D scene representations like Neural Radiance Fields [32] (NeRF) and 3D Gaussian Splatting [19] (3DGS) to enable *pose-agnostic* SCD from unconstrained viewpoints. Complementary efforts [8, 13, 20] explore *label-free* SCD to remove the reliance on costly and labor-intensive human-labeled changes, improving robustness under domain and data distribution shifts.

Despite recent advances, state-of-the-art (SOTA) SCD

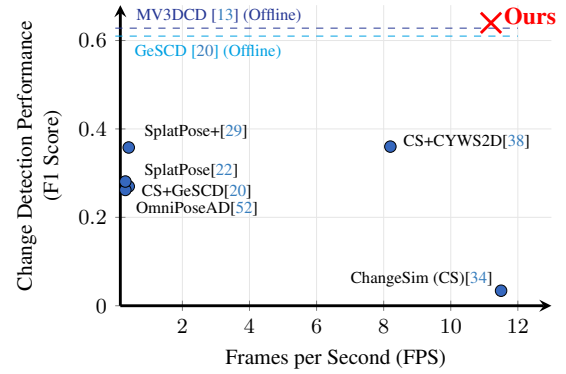


Figure 1. Our *online* scene change detection method establishes a new state of the art, detecting changes more reliably than all prior methods, including the strongest *offline* baselines. It operates at a runtime comparable to the fastest *online* approaches while achieving substantially higher F1 scores.

methods [13, 20, 30] are confined to an *offline* setting, where both pre- and post-change observations are available prior to inference. In contrast, *online* change inference—referred to as *online SCD*—detects changes on the fly as new images are acquired during a scene revisit, without access to future observations. This setting is critical for real-time decision-making and intervention in embodied and robotic systems. As in prior *online* approaches [22, 29, 34, 34], we assume that the scene remains static within each revisit. As shown in Fig. 1, existing *online* SCD methods exhibit a substantial accuracy gap compared to SOTA *offline* approaches. Moreover, many fail to sustain real-time performance, limiting their practical applicability.

We introduce a novel SCD approach that, for the first time, unifies the strengths of *online*, *pose-agnostic*, and *label-free* methods, while additionally enforcing *multi-view consistency* [13] during inference. Our method surpasses existing *online* and *offline* methods in detection performance while operating at over 10 FPS. This leap in both speed and accuracy is enabled by two key algorithmic and system-level innovations: a novel self-supervised loss enforcing change information consistency across viewpoints,

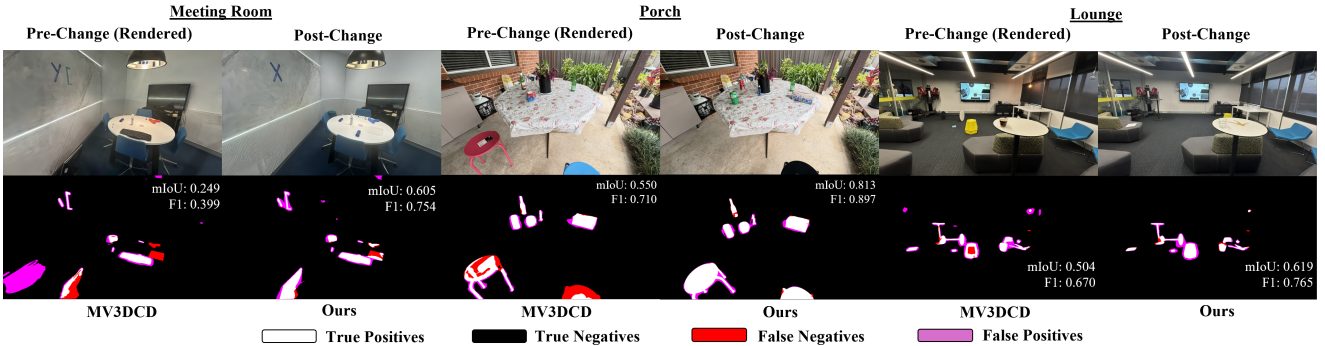


Figure 2. Qualitative comparison with MV3DCD [13]. MV3DCD’s hard thresholding and intersection heuristic lead to missed or spurious detections, especially for subtle appearance changes in semantically similar objects (red-to-blue T-shaped object in Meeting Room, blue-to-black bench in Porch). Hard thresholding risks discarding subtle but important changes, while the intersection fails to capture true changes unless present in both masks. Our method jointly learns complementary change information in pixel- and feature-level cues via our novel self-supervised loss, capturing fine-grained changes and achieving state-of-the-art performance in both online and offline settings.

addressing the limitations of hard-thresholded intersection fusion [13] (see Fig. 2), and an ultra-light PnP-based pose estimation module.

Our third innovation is a change-guided update strategy for the 3DGGS-based scene representation. Maintaining an up-to-date representation of an evolving scene without naively reconstructing it from scratch is challenging [1, 5, 7, 51], but essential for long-term monitoring. Naïve reconstruction after each inspection round is computationally expensive and discards well-reconstructed information from unchanged regions. We address this by leveraging the predicted change masks to guide selective updates: only changed regions are newly reconstructed, fused with existing primitives, and refined through a lightweight global adjustment while preserving the geometry and the appearance of unchanged areas. Our selective update approach enables scene representation updates in seconds while reusing the high-fidelity representations of unchanged regions.

In summary, we make three contributions validated by our extensive experiments across real-world environments:

- We present an online approach for pose-agnostic SCD from unposed monocular images, operating in real time. Our approach is label-free and multi-view.
- We propose a novel self-supervised loss that jointly integrates feature- and pixel-level cues without heuristic fusion or hard-thresholding, achieving state-of-the-art performance in both online and offline settings.
- We introduce a change-guided selective reconstruction and fusion strategy that enables efficient, repeatable scene representation updates within seconds.

2. Related Work

2.1. Scene Change Detection

SCD has traditionally been studied as a bitemporal pairwise problem, where a model detects changes between

two images captured at two time instances from identical [2, 6, 9, 25, 40, 47] or closely-aligned [27, 38, 39] viewpoints. Most approaches formulate this as a segmentation task [2, 6, 9, 27, 40], while few explore bounding box prediction [38, 39], relying fully [2, 6, 9, 25, 27, 38–40, 47] or partially [24, 41] on costly human annotations to compensate for lighting variations, seasonal changes, or viewpoint inconsistencies. However, this paradigm has clear limitations: performance degrades under distribution shifts, annotation is tedious, and the range of possible changes in complex scenes is virtually unbounded. Recent work [3, 8, 13, 18, 20] has shifted toward label-free or zero-shot approaches, driven by the emergence of powerful visual foundation models [21, 33]. However, these methods [3, 8, 18, 20] assume image pairs with identical viewpoints are available—a condition rarely satisfied in autonomous systems operating along independent trajectories, and a condition we do not assume.

More recent methods [13, 17, 30] exploit high-fidelity 3D scene representations [19, 48] to model the pre-change scene and render novel views from post-change viewpoints, motivating pose-agnostic SCD. MV3DCD [13] showed that learning change information across multiple viewpoints with a scene representation significantly outperforms pairwise predictions. However, these approaches require a complete set of pre- and post-change captures, and use Structure-from-Motion [45] (SfM) to register poses to a common reference frame, confining them to an offline setting. In contrast, we study SCD in an online and incremental regime, where changes are inferred on-the-fly.

Pose-agnostic anomaly detection [22, 29, 52] also builds a 3D representation of a pre-change object. To detect anomalies, the object is rendered from the post-change viewpoint, then scored using feature comparisons. However, these works focus on single objects rather than large-scale scenes. Approaches such as [22, 52] optimize camera

poses directly against the representation, leading to slower pose estimation and, as shown by MV3DCD [13], frequent convergence failures in large complex scenes with multiple changes and view-dependent inconsistencies. Liu *et al.* [29] improved efficiency by replacing this step with HLoc [42].

While also employing a self-supervised objective, the approach of Furukawa *et al.* [12] differs fundamentally from our formulation of the self-supervised loss. Their loss is designed to exclude high-error regions to facilitate 2D alignment, whereas ours instead integrates complementary yet potentially noisy change cues across modalities into a persistent 3D representation.

ChangeSim [34] also investigates online SCD. However, ChangeSim depends on an off-the-shelf RGB-D SLAM system [23] for pose estimation and assumes that pre- and post-change trajectories are closely aligned. This reduces the task to image retrieval, where the nearest pre-change view (by L_1 distance between camera poses) is selected. In contrast, we make no assumptions about incoming RGB-only frames or the trajectories; instead, we estimate poses directly in the pre-change coordinate frame and infer change masks by jointly leveraging all viewpoints observed so far. Our approach operates fully *label-free*, *pose-agnostic*, *multi-view*, *online*, and at *real-time* rates.

2.2. Efficient Representation Update

NeRFs [32] and 3DGS [19] are widely adopted photorealistic scene representations, capturing fine geometry and appearance. NeRFs regress a 5D plenoptic function [4] using an MLP network to parameterize density and view-dependent radiance, while 3DGS employs anisotropic Gaussian primitives for real-time novel-view-synthesis.

Recently, there has been growing interest in real-time reconstruction [28, 31]. However, these methods generally underperform compared to offline counterparts and require substantial view overlap between frames. In contrast, approaches that address the long-term evolution of scenes remain less explored, focusing on updating representations from sparse and intermittent captures [1, 49]. Closely related is continual learning for photorealistic scene representations [1, 5, 49, 51]. NeRF-based continual learning approaches [5, 49] utilize distillation or generative replay but inherit slow inference and longer optimization times. GaussianUpdate [51] proposes a three-stage optimization pipeline requiring substantial training iterations. CL-Splats [1] introduces a local optimization kernel to calculate gradients only for changed primitives, yet cannot robustly handle global appearance variations, particularly the illumination shifts often present between real-world inspection scenarios.

Long-term scene representations are also well-explored in robotics for autonomous navigation. To maintain spatial consistency in dynamic environments, these systems uti-

lize volumetric representations [11, 43], object-aware tracking [36, 53], unified metric-semantic frameworks [44], and recently, 3DGS [50].

Continual learning approaches [1, 5, 49, 51] focus on updating representations while facilitating history recovery. In contrast, we focus on updating the representation with minimal training overhead, enabling frequent repeated inspections. To this end, we propose a simple selective modeling strategy that only reconstructs changed regions, guided by our change masks and the change representation, followed by fusion with existing primitives. A lightweight global optimization step ensures consistency, enabling updates within seconds while robustly handling both geometric and appearance changes, including global illumination variations.

3. Methodology

Our approach is illustrated in Fig. 3. We begin by constructing a 3DGS [19] representation of the pre-change (*reference*) scene offline (Sec. 3.1). Incoming images of the post-change (*inference* scene) are processed online. We estimate its pose relative to the reference scene (Sec. 3.2), then render the corresponding viewpoint to extract change cues (Sec. 3.3). These cues are used to infer a change mask (Sec. 3.4), leveraging current and previous observations. After processing all observations, the representation is updated (Sec. 3.5) to the current state of the environment.

Problem Setup: The reference scene \mathcal{R}_{ref} is captured with a set of n_{ref} images, $\mathcal{I}_{\text{ref}} = \{I_{\text{ref}}^k\}_{k=1}^{n_{\text{ref}}}$. Over time, the scene undergoes changes in structure (e.g., additions, removals, or object movement), or object appearance (e.g., variations in color or texture), forming the inference scene \mathcal{R}_{inf} . In addition, there may be ‘distractors’ such as reflections, shadows and global illumination changes.

Our objective is to generate a binary change segmentation mask M^k for each incoming inference frame I_{inf}^k that localizes all relevant changes between \mathcal{R}_{ref} and \mathcal{R}_{inf} while suppressing distractors. After processing all inference frames $\mathcal{I}_{\text{inf}} = \{I_{\text{inf}}^k\}_{k=1}^{n_{\text{inf}}}$, we obtain a set of refined masks $\mathcal{M} = \{M_{\text{refined}}^k\}_{k=1}^{n_{\text{inf}}}$. Using the change masks \mathcal{M} together with \mathcal{I}_{inf} , we selectively update the reference representation \mathcal{R}_{ref} to reflect the scene’s current state \mathcal{R}_{inf} .

3.1. Building Reference Scene Representation

Following the standard 3DGS pipeline [19], we first estimate the camera poses $\mathcal{P}_{\text{ref}} = \{P_{\text{ref}}^k\}_{k=1}^{n_{\text{ref}}}$ for all images in \mathcal{I}_{ref} using SfM [45]. Using \mathcal{I}_{ref} , \mathcal{P}_{ref} and a sparse point cloud from SfM, we construct the \mathcal{R}_{ref} with Speedy-Splat [15]. We assume that the viewpoints, scene coverage, and image quality in \mathcal{I}_{ref} are sufficient to produce a high-fidelity \mathcal{R}_{ref} .

3.2. Inferring Pose of an Incoming Frame

For each reference image $I_{\text{ref}}^k \in \mathcal{I}_{\text{ref}}$, we extract keypoints and descriptors using XFeat [35] as a fast, lightweight de-

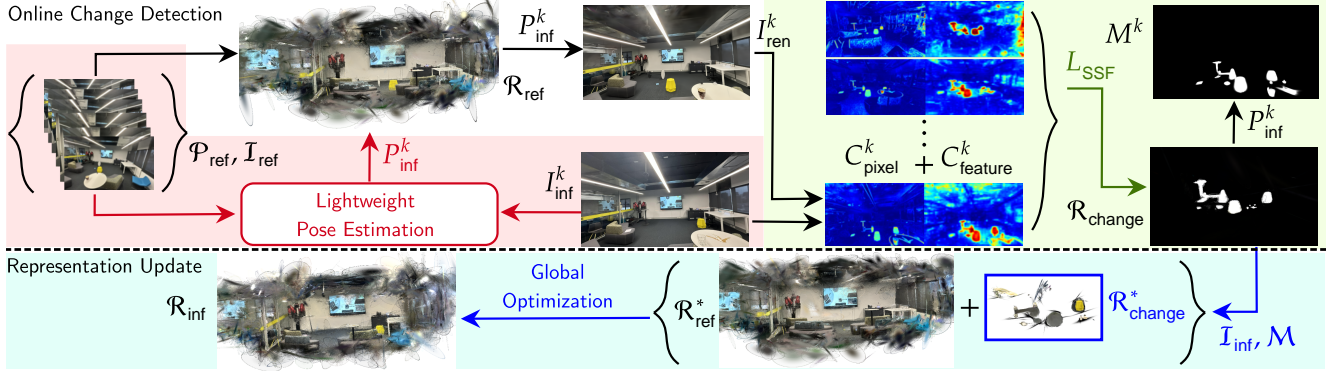


Figure 3. Proposed approach with this paper’s contributions highlighted. We register an incoming inference image I_{inf}^k to an existing reference representation \mathcal{R}_{ref} with a **lightweight PnP-based pose estimator**. Using the estimated pose P_{inf}^k and \mathcal{R}_{ref} to render an aligned image I_{ren}^k , we extract change cues C^k as a combination of pixel- and feature-level cues. Our novel **self-supervised fusion loss** L_{SSF} guides the fusion of all observed change cues to build a change representation $\mathcal{R}_{\text{change}}$ that collectively learns change information from multiple viewpoints and infer change masks M^k . Finally, we **selectively reconstruct changed regions** to update the representation to \mathcal{R}_{inf} .

tector, followed by exhaustive matching across all reference images. Using the known camera poses \mathcal{P}_{ref} , these correspondences are triangulated to form a consistent 3D point set associated with each I_{ref}^k . This point set serves as a geometric anchor for estimating the pose of incoming inference frames by establishing 2D–3D correspondences between their detected keypoints and the reference points.

Given an incoming frame I_{inf}^k , we extract its descriptors and select the top- n reference frames with the highest number of matches ($n = 4$ in our experiments). These reference frames provide candidate 2D–3D correspondences, which are then used to estimate the pose P_{inf}^k of I_{inf}^k via PnP with RANSAC [10, 26]. Finally, we refine P_{inf}^k with inliers through a GPU-parallel miniBA [31].

Since pose estimation for I_{inf}^k relies exclusively on the retrieved reference frames, the system operates without drift accumulation. Moreover, by restricting inference to a fixed-size set of reference frames, we achieve constant-time $O(1)$ pose estimation. We discuss some limitations of the XFeat features in the supplementary material.

3.3. Extracting Change Cues

With P_{inf}^k expressed in the coordinate frame of \mathcal{P}_{ref} , we query \mathcal{R}_{ref} to render the corresponding pre-change view I_{ren}^k , matching the viewpoint of the incoming frame I_{inf}^k . For the image pair $(I_{\text{inf}}^k, I_{\text{ren}}^k)$, we extract change cues by computing differences at both the pixel and feature levels, capturing both appearance and structural changes.

Pixel-level change cues: We quantify the differences between $(I_{\text{inf}}^k, I_{\text{ren}}^k)$ at the pixel level using a combination of L_1 and D-SSIM terms, following the photometric error formulation in 3DGS [19] (Eq. 1) with $\lambda = 0.2$ following 3DGS [19]. We normalize C_{pixel}^k to $[0, 1]$.

$$C_{\text{pixel}}^k = (1 - \lambda)L_1 + \lambda L_{\text{D-SSIM}}. \quad (1)$$

Feature-level change cues: To capture high-level semantic differences, we leverage the visual foundation model SAM2-Tiny [37] to extract dense feature maps $(f_{\text{inf}}^k, f_{\text{ren}}^k)$ for $(I_{\text{inf}}^k, I_{\text{ren}}^k)$. Each feature map is represented as $f \in \mathbb{R}^{\frac{h}{s} \times \frac{w}{s} \times d}$, where h and w denote the image height and width, s is the patch size, and d is the feature dimensionality. The feature-level change cues C_{feature}^k are computed as the absolute difference between the two feature maps:

$$C_{\text{feature}}^k = \sum_{i=1}^d |f_{\text{inf}}^{k,i} - f_{\text{ren}}^{k,i}| \in \mathbb{R}^{\frac{h}{s} \times \frac{w}{s}}, \quad (2)$$

followed by bilinear interpolation to the original image resolution (h, w) and normalization to the range $[0, 1]$.

Combined change cues: The final change cue map C^k for each I_{inf}^k combines pixel- and feature-level cues through simple addition ($C^k = C_{\text{pixel}}^k + C_{\text{feature}}^k$) balancing low-level appearance differences with high-level semantic variations.

This formulation leverages the complementary strengths of pixel- and feature-level cues while avoiding the loss of change information. Pixel-level cues effectively capture fine-grained appearance differences, such as color variations between semantically similar objects, but tend to be more sensitive to distractor changes caused by shadows, reflections, or illumination shifts. Feature-level cues are more robust to these distractors yet may struggle to detect subtle differences within semantically similar regions. MV3DCD [13] relies on hard thresholding, which can disregard subtle but relevant changes that fall below predefined thresholds. Moreover, since MV3DCD fuses its structure and feature-aware masks through intersection, it may further lose valid change information not simultaneously captured by both masks. When combined with our novel self-supervised fusion loss (Sec. 3.4), the proposed formulation jointly integrates information across all observed

viewpoints, effectively suppressing inconsistent distractors while maintaining sensitivity to meaningful changes.

3.4. Inferring Change Masks

MV3DCD [13] first enforced multi-view consistency for SCD using 3DGS [19]. We depart from its hard-thresholded heuristic fusion and introduce a novel self-supervised loss that jointly infers multi-view consistent change masks from all observed cues at test time.

After the reference scene \mathcal{R}_{ref} is constructed (Sec. 3.1), we initialize the *change* representation $\mathcal{R}_{\text{change}}$ from \mathcal{R}_{ref} by discarding all color parameters and introducing a learnable change parameter c [13] for each primitive.

$\mathcal{R}_{\text{change}}$ serves two purposes: (1) it enables fusing change cues C^k from any viewpoint into a single, multi-view consistent change representation, and (2) it acts as a persistent memory that carries change information over observing viewpoints. As a result, when a new frame arrives, the incoming change cues are fused with all previously observed cues in $\mathcal{R}_{\text{change}}$. Rendering $\mathcal{R}_{\text{change}}$ at the pose P_{inf}^k yields the predicted change mask M^k for that viewpoint.

For an incoming I_{inf}^k , before inferring the change mask M^k , we update $\mathcal{R}_{\text{change}}$ for n iterations ($n = 16$ in our experiments) using our self-supervised fusion loss:

$$L_{\text{SSF}} = C^i \odot (1 - \tilde{M}^i) + \log(1 + \text{mean}(\tilde{M}^i)^2), \quad (3)$$

where \odot denotes Hadamard (i.e. element-wise) multiplication and \tilde{M}^i is the sigmoid-activated rendered change mask $\sigma(M_{\text{ref}}^i)$ from the viewpoint of the i -th frame. At each iteration, we randomly sample i from all past inference frame IDs $i \in [0, k]$, but biased towards the most recent frame k with $1/3$ probability. C^i contains the combined change cues of the i -th frame (Sec. 3.3). We infer the change mask M^k for the k^{th} frame after this optimization.

Intuitively, minimizing L_{SSF} encourages the change parameters \tilde{c} in $\mathcal{R}_{\text{change}}$ to change so that the rendered \tilde{M}^i has values close to 1 in regions where change cues are strong via the term $C^i \odot (1 - \tilde{M}^i)$. To prevent the trivial solution of $\tilde{M}^i = 1$ everywhere, the regularization term $\log(1 + \text{mean}(\tilde{M}^i)^2)$ is included.

This formulation allows us to infer M^k for I_{inf}^k jointly from all past and current change cues. By accumulating change information from all observed frames in $\mathcal{R}_{\text{change}}$, we enforce multi-view consistency and mitigate view-dependent distractors from irrelevant changes.

3.5. Scene Representation Update

After completing online change detection for all observations, we perform a post-refinement of $\mathcal{R}_{\text{change}}$ using all C^k , and render refined change masks M_{refined}^k for $k \in [0, n_{\text{inf}}]$.

We then discard c from each primitive in $\mathcal{R}_{\text{change}}$ and introduce view-dependent appearance modeled via spherical harmonics [19]. To only reconstruct changed regions, we

mask the inference images using the refined change masks as $\hat{I}_{\text{inf}}^k = I_{\text{inf}}^k \odot M_{\text{refined}}^k$. \hat{I}_{inf}^k guides the reconstruction of changed regions $\mathcal{R}_{\text{change}}^*$ following the standard 3DGS [19] optimization pipeline. This disentangled reconstruction is highly efficient and requires a fraction of the primitives compared to modeling the entire scene, thereby accelerating rendering and avoiding redundant computations in unchanged regions. Notably, this selective reconstruction achieves rendering speeds exceeding 400 FPS, substantially reducing overall optimization time.

Next, we fuse $[\mathcal{R}_{\text{ref}}^*, \mathcal{R}_{\text{change}}^*]$ to form the inference scene \mathcal{R}_{inf} , where $\mathcal{R}_{\text{ref}}^*$ denotes \mathcal{R}_{ref} excluding primitives that contribute to changed pixels. A fast global optimization is then performed, guided by \mathcal{I}_{inf} . We restrict the adaptive density control [19] only to the primitives contributing to changed pixels in at least one view to avoid unnecessary densification in unchanged regions.

This restricted global refinement serves multiple purposes: (1) it accounts for global illumination differences, (2) it mitigates boundary artifacts that may arise around the changed regions after fusion, and (3) it corrects residual errors due to imperfect change masks. Our design reuses primitives from \mathcal{R}_{ref} wherever possible, while $\mathcal{R}_{\text{change}}^*$ efficiently models new structures. Together, these design choices significantly speed up optimization, enabling complete scene updates within seconds.

4. Experiments

Datasets: We evaluate our method on PASLCD [13] for SCD. PASLCD comprises 10 room-scale (i.e., a cantina) indoor and outdoor scenes captured under similar and varying lighting conditions. It features both surface-level appearance and object-level geometric changes, along with numerous distractors such as shadows, reflections, and illumination shifts, making it a highly challenging multi-view dataset for SCD. Importantly, PASLCD captures scenes from unconstrained, independently traversed camera trajectories, closely reflecting real-world autonomous operation. For the scene representation update, we evaluate on PASLCD [13] and CL-Splats [1]. CL-Splats consists of five small-scale (i.e., tabletop) scenes, each featuring a single object-level change.

Baselines and Metrics: We conduct a comprehensive evaluation using the best-performing baselines [8, 13, 20, 22, 27, 29, 30, 34, 38, 52]. For pairwise methods [8, 20, 27, 30, 38] evaluated in the offline setting, we render identical viewpoints using vanilla 3DGS [19] for a fair comparison, although this substantially simplifies the task by removing viewpoint inconsistencies. For the online setting, we construct two additional baselines by integrating ChangeSim’s [34] frame matching with the best-performing pairwise methods [20, 38]. We provide ground-truth poses for ChangeSim’s frame retrieval module to ensure a fair eval-

Table 1. Quantitative results for SCD on PASLCD [13] averaged over all 20 instances. LF: Label-Free, PA: Pose-Agnostic, MV: Multi-View consistency for change detection, ON: Online. We additionally report the total runtime, including pose estimation and reference reconstruction, for offline methods, and the operating frame rate (FPS) for online methods. Our method achieves the best performance in both settings, even outperforming all existing offline methods while operating online.

Method	LF	PA	MV	ON	mIoU	F1	Runtime / FPS
R-SCD [27]	–	–	–	–	0.118	0.199	194s
CYWS2D [38]	–	–	–	–	0.273	0.398	189s
GeSCD [20]	✓	–	–	–	0.477	0.611	298s
ZeroSCD [8]	✓	–	–	–	0.306	0.414	409s
3DGSCD [30]	✓	✓	✓	–	0.209	0.339	824s
MV3DCD [13]	✓	✓	✓	–	0.478	0.628	479s
Ours (Offline)	✓	✓	✓	–	0.552	0.694	156s
ChangeSim (CS) [34]	–	–	–	✓	0.018	0.034	11.5
CS+CYWS2D [38]	–	–	–	✓	0.243	0.360	8.2
CS+GeSCD [20]	✓	–	–	✓	0.181	0.270	<1
OmniposeAD [52]	✓	✓	–	✓	0.168	0.262	<1
SplatPose [22]	✓	✓	–	✓	0.173	0.281	<1
SplatPose+ [29]	✓	✓	–	✓	0.237	0.358	<1
Ours	✓	✓	✓	✓	0.486	0.638	11.2

uation, as PASLCD lacks depths for ChangeSim’s off-the-shelf RGB-D SLAM system. We use model checkpoints provided by the authors for the supervised methods [27, 38]. Following standard practice in SCD [2, 13, 27, 41], we report mean intersection over union (mIoU) and F1 score computed for change pixels in the ground-truth mask.

For efficient scene representation update, we adopt 3DGS and fast variants [15, 16, 19] as our baselines. We also evaluate CLNeRF [5] among publicly available continual learning methods. Following standard evaluation protocols [1, 5, 19, 49, 51], we report PSNR, SSIM, and LPIPS for novel views after scene update, along with runtimes.

4.1. Experiments on Scene Change Detection

Offline SCD Results: Table 1 presents an extensive comparison against SOTA methods across all SCD settings on PASLCD [13]. In the offline setting, we follow the protocol of MV3DCD [13] by optimizing $\mathcal{R}_{\text{change}}$ using our L_{SSF} with access to all inference views jointly for 3k iterations.

Generally, label-free approaches yield better performance. Among these, our method achieves the highest overall performance, improving mIoU by approximately **15%** over the strongest offline competitor, MV3DCD, while running nearly **3× faster**. The SCD performance gain primarily stems from our proposed self-supervised fusion loss L_{SSF} , which eliminates the hard thresholding and intersection heuristics used in MV3DCD, enabling more robust and

Table 2. Runtime analysis of each module in our online SCD pipeline, measured in milliseconds per frame on PASLCD [13]. Most of the computation time is spent on multi-view change information fusion, while other modules are lightweight.

Module	ms/Frame	Percentage (%)
Extracting Descriptors	1.28	1.4
Reference Image Retrieval	11.50	12.8
Pose Estimation	16.47	18.4
Change Cue Generation	1.69	1.9
Multi-View Change Cue Fusion	58.17	64.9
Change Mask Inference	0.49	0.6
Total	89.60	100

fine-grained change localization.

Online SCD Results: We compare our approach with existing online SCD methods (Table 1). In the online setting, our approach achieves **2× higher mIoU** than the strongest competitor, CS+CYWS2D [38], while maintaining real-time performance at **11 FPS**. Notably, SOTA offline methods such as GeSCD [20] experience severe degradation when exposed to viewpoint discrepancies. CYWS2D exhibits a smaller performance drop under such conditions, likely due to its pretraining on COCO-Inpainted [38], which includes image pairs with viewpoint variations. The upper bounds of these two methods under identical viewpoints are shown in the offline setting. Remarkably, our online approach not only establishes SOTA results among online methods but also surpasses the best offline models, demonstrating strong robustness and efficiency under real-world conditions. We conduct all experiments at 1008×560 resolution on a GeForce RTX4090. FPS was measured as empirical wall-clock time over the number of frames processed.

Runtime Analysis: Table 2 summarizes the runtime breakdown (asynchronous overhead) of our online SCD pipeline for a single inference frame I_{inf}^k . Approximately 33% of the total time is spent on pose estimation, aligning I_{inf}^k to the

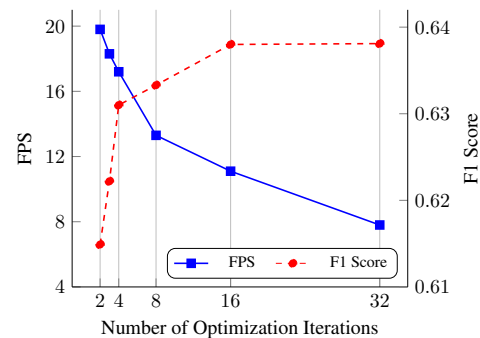


Figure 4. Speed–accuracy trade-off of our online method. Our method can operate between 11–20 FPS with a relative performance drop of 3.6% in F1 Score.

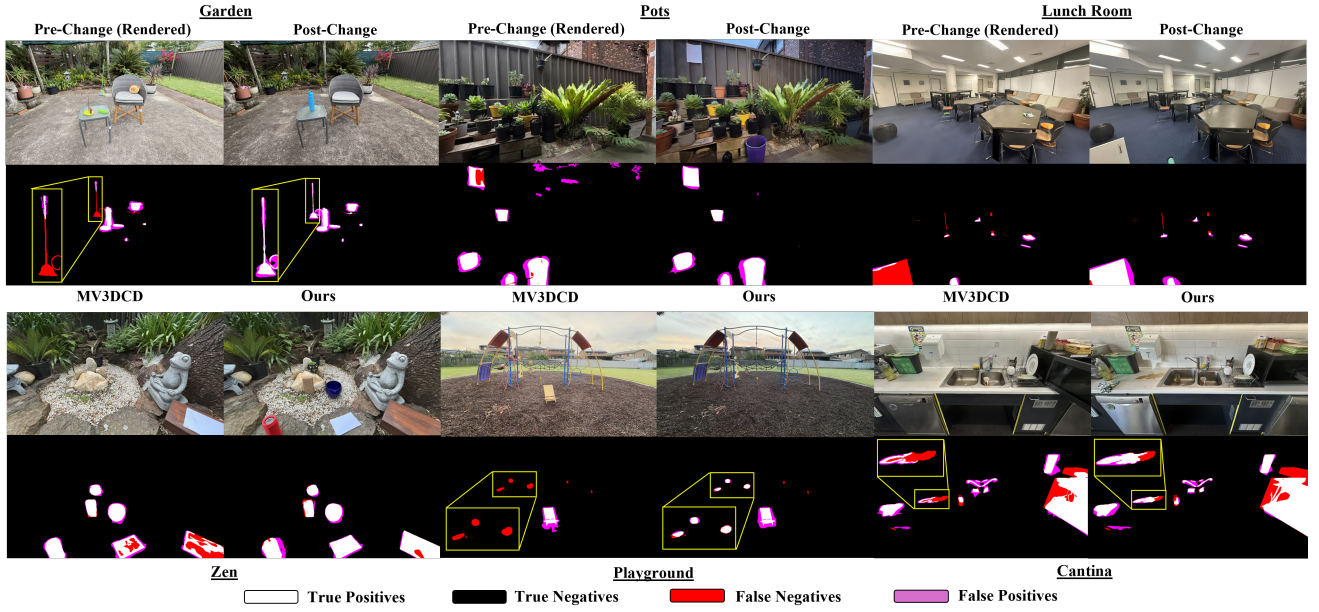


Figure 5. Additional qualitative comparison with MV3DCD [13]. Our rendered change masks align more closely with the ground truth, capturing subtle structural and appearance changes that MV3DCD often misses. In contrast to MV3DCD, our method produces fewer spurious detections and demonstrates strong robustness to distractor variations across both indoor and outdoor environments.

coordinate system of \mathcal{R}_{ref} . SCD accounts for 67% of the overall runtime, of which the majority (94%) is attributed to multi-view change cue fusion spent on optimizing $\mathcal{R}_{\text{change}}$.

Speed Vs. Accuracy Trade-off: We vary the number of iterations used for multi-view change cue fusion—the dominant contributor to runtime (Fig. 4). Our approach can operate between 11–20 FPS, with only a modest 3.6% drop in F1 score. This efficiency stems from $\mathcal{R}_{\text{change}}$, which serves as a persistent memory of previously learned changes, minimizing the iterations needed for subsequent frames.

Qualitative Results: We present qualitative comparisons against our closest competitor, MV3DCD [13], in Figs. 2 and 5. Our method demonstrates superior change localization and robustness across diverse real-world scenes. Unlike MV3DCD, our approach produces cleaner and more spatially coherent change masks with significantly fewer false negatives. It effectively captures subtle appearance and geometric changes that MV3DCD often overlooks, while suppressing false positives caused by distractors. These results highlight that our self-supervised fusion of pixel- and feature-level cues combined with multi-view consistency enables accurate, fine-grained change detection.

Ablation Analysis: We conduct an ablation study on PASLCD [13] (Table 3). Removing either the L_1 or $L_{\text{D-SSIM}}$ term in C_{pixel} noticeably degrades performance, with the former providing a relatively stronger supervisory signal for L_{SSF} . When using either C_{pixel} or C_{feature} , the model fails to converge, indicating that neither modality alone sufficiently guides L_{SSF} . Removing the regularization term collapses

Table 3. Ablation study of our SCD approach on PASLCD [13]. Performance benefits from every component.

Variant	mIoU ↑	F1 ↑
Ours (Full)	0.486	0.638
– L_1	0.320	0.464
– $L_{\text{D-SSIM}}$	0.447	0.620
– C_{pixel} (using only C_{feature})	✗	✗
– C_{feature} (using only C_{pixel})	✗	✗
– Regularization term	✗	✗
Ours (With [13]'s Thresholding & Heuristic Fusion)	0.350	0.495

training into the trivial solution $\tilde{M}^k = 1$ (discussed in sec. 3.4). Using MV3DCD's [13] hard thresholding and intersection heuristic instead of L_{SSF} degrades performance.

4.2. Experiments on 3DGS Representation Update

Quantitative Results: We compare our change-guided representation update strategy against reconstructing the scene from scratch [15, 16, 19] and updating [5] in Table 4. Our method achieves comparable or slightly superior performance while substantially reducing the training overhead. For example, total optimization time is **8× faster** than 3DGS-LM [16] and **13× faster** than 3DGS [19] on PASLCD [13]. The slight performance gain arises from reusing the well-reconstructed, unchanged regions of the reference scene, which may not be well captured by the limited set of inference views.

Table 4. Quantitative comparison of scene representation update on PASLCD [13] and CL-Splats [1]. Our method achieves comparable or higher reconstruction quality than approaches that fully re-optimize the evolved scene from scratch, while providing updated representations within seconds (< 60s), achieving up to **8–9× faster** runtimes. Results are averaged over all instances and scenes.

Method	PASLCD				CL-Splats			
	PSNR (dB) \uparrow	SSIM \uparrow	LPIPS \downarrow	Runtime (s) \downarrow	PSNR (dB) \uparrow	SSIM \uparrow	LPIPS \downarrow	Runtime (s) \downarrow
3DGS [19]	22.21	0.7558	0.2426	550	30.31	0.9319	0.1178	364
3DGS-LM [16]	22.26	0.7562	0.2422	340	29.95	0.9322	0.1177	275
SpeedySplats [15]	22.25	0.7603	0.2618	399	29.89	0.9349	0.1290	312
CLNeRF [5]	22.27	0.6239	0.3907	451	26.29	0.7867	0.2235	301
Ours	23.70	0.7868	0.2491	42	30.54	0.9356	0.1256	39



Figure 6. Qualitative comparison of rendered views from the updated representation with CLNeRF [5] and 3DGS [19] (from scratch). Our method more accurately reconstructs changed regions (red boxes) while reusing primitives from \mathcal{R}_{ref} to preserve high fidelity in unchanged areas (yellow boxes), compared to naïve reconstruction at each time.

Table 5. Analysis on scene update component on PASLCD [13]. Runtime for change detection and refinement is excluded. GO: Global Optimization, SR: Selective Reconstruction.

Variant	PSNR (dB) \uparrow	SSIM \uparrow	LPIPS \downarrow	Runtime (s) \downarrow
GO Only (3DGS)	22.64	0.7611	0.2550	145
GO Only (Ours)	23.01	0.7751	0.2553	79
SR Only	19.89	0.6814	0.3084	28
Ours (Full)	23.70	0.7868	0.2491	36

Qualitative Results: We present qualitative comparisons with 3DGS [19] and CLNeRF [5] in Fig. 6. Our method more accurately reconstructs the changed regions compared to CLNeRF, while also achieving higher visual fidelity in unchanged areas than 3DGS (built from scratch), owing to the effective reuse of primitives from the reference scene.

Ablation Analysis: To evaluate runtime efficiency (Table 5), all experiments are conducted for 10k iterations. We begin with standard global optimization following 3DGS’s adaptive density control [19]. Restricting this process to primitives associated with changed pixels accelerates train-

ing by avoiding densification in unchanged regions. Selective reconstruction alone runs approximately **5× faster** than standard global optimization but introduces local artifacts when used in isolation (discussed in Sec. 3.5). Combining selective reconstruction with our global optimization achieves the best of both approaches, where the former efficiently models new geometry while the latter corrects residual artifacts locally and illumination differences globally.

5. Conclusion

We proposed a novel approach to pose-agnostic SCD that detects change in an online manner with SOTA performance, outperforming even the best offline methods. We introduce two key algorithmic and system-level innovations to achieve this: an ultra-light PnP-based pose estimator and a self-supervised fusion loss for learning a multi-view consistent change representation. Additionally, we introduced a change-guided update strategy for 3DGS, reducing training overhead to seconds while retaining reconstruction fidelity. Future work may focus on developing richer complementary change cues, potentially improving both online and offline SCD performance.

6. Acknowledgment

This work was supported by the Australian Research Council Research Hub in Intelligent Robotic Systems for Real-Time Asset Management (ARIAM) (IH210100030) and Abyss Solutions. C.J., N.S., and D.M. also acknowledge ongoing support from the QUT Centre for Robotics.

References

- [1] Jan Ackermann, Jonas Kulhanek, Shengqu Cai, Xu Haofei, Marc Pollefeys, Gordon Wetzstein, Leonidas Guibas, and Songyou Peng. CL-Splats: Continual learning of Gaussian splatting with local optimization. In *Proceedings of the IEEE/CVF International Conference on Computer Vision (ICCV)*, 2025. [2](#), [3](#), [5](#), [6](#), [8](#)
- [2] Pablo F Alcantarilla, Simon Stent, German Ros, Roberto Arroyo, and Riccardo Gherardi. Street-view change detection with deconvolutional networks. *Autonomous Robots*, 42(7):1301–1322, 2018. [2](#), [6](#)
- [3] Tim Alpherts, Sennay Ghebreab, and Nanne van Noord. EM-PLACE: Self-supervised urban scene change detection. In *Proceedings of the AAAI Conference on Artificial Intelligence*, pages 1737–1745, 2025. [2](#)
- [4] James R Bergen and Edward H Adelson. The plenoptic function and the elements of early vision. *Computational models of visual processing*, 1(8):3, 1991. [3](#)
- [5] Zhipeng Cai and Matthias Müller. CINeRF: Continual learning meets Nerf. In *Proceedings of the IEEE/CVF International Conference on Computer Vision*, pages 23185–23194, 2023. [2](#), [3](#), [6](#), [7](#), [8](#)
- [6] Shuo Chen, Kailun Yang, and Rainer Stiefelhagen. DRTANet: dynamic receptive temporal attention network for street scene change detection. In *2021 IEEE Intelligent Vehicles Symposium (IV)*, pages 502–509. IEEE, 2021. [2](#)
- [7] Luqi Cheng, Zhangshuo Qi, Zijie Zhou, Chao Lu, and Guangming Xiong. LT-Gaussian: Long-term map update using 3D Gaussian splatting for autonomous driving. In *2025 IEEE Intelligent Vehicles Symposium (IV)*, pages 1427–1433. IEEE, 2025. [2](#)
- [8] Kyusik Cho, Dong Yeop Kim, and Euntai Kim. Zero-shot scene change detection. In *Proceedings of the AAAI Conference on Artificial Intelligence*, pages 2509–2517, 2025. [1](#), [2](#), [5](#), [6](#)
- [9] Rodrigo Caye Daudt, Bertr Le Saux, and Alexandre Boulch. Fully convolutional siamese networks for change detection. In *2018 25th IEEE international conference on image processing (ICIP)*, pages 4063–4067. IEEE, 2018. [2](#)
- [10] Martin A Fischler and Robert C Bolles. Random sample consensus: A paradigm for model fitting with applications to image analysis and automated cartography. *Communications of the ACM*, 24(6):381–395, 1981. [4](#)
- [11] Jiahui Fu, Chengyuan Lin, Yuichi Taguchi, Andrea Cohen, Yifu Zhang, Stephen Mylabathula, and John J Leonard. Planesdf-based change detection for long-term dense mapping. *IEEE Robotics and Automation Letters*, 7(4):9667–9674, 2022. [3](#)
- [12] Yukuko Furukawa, Kumiko Suzuki, Ryuhei Hamaguchi, Masaki Onishi, and Ken Sakurada. Self-supervised simultaneous alignment and change detection. In *2020 IEEE/RSJ International Conference on Intelligent Robots and Systems (IROS)*, pages 6025–6031, 2020. [3](#)
- [13] Chamuditha Jayanga Galappaththige, Jason Lai, Lloyd Windrim, Donald Dansereau, Niko Sunderhauf, and Dimity Miller. Multi-view pose-agnostic change localization with zero labels. In *Proceedings of the Computer Vision and Pattern Recognition Conference*, pages 11600–11610, 2025. [1](#), [2](#), [3](#), [4](#), [5](#), [6](#), [7](#), [8](#)
- [14] Dongyeob Han, Suk Bae Lee, Mihwa Song, and Jun Sang Cho. Change detection in unmanned aerial vehicle images for progress monitoring of road construction. *Buildings*, 11(4):150, 2021. [1](#)
- [15] Alex Hanson, Allen Tu, Geng Lin, Vasu Singla, Matthias Zwicker, and Tom Goldstein. Speedy-Splat: Fast 3D Gaussian splatting with sparse pixels and sparse primitives. In *Proceedings of the Computer Vision and Pattern Recognition Conference (CVPR)*, pages 21537–21546, 2025. [3](#), [6](#), [7](#), [8](#)
- [16] Lukas Höllerin, Aljaž Božič, Michael Zollhöfer, and Matthias Nießner. 3DG-S-LM: Faster Gaussian-splatting optimization with Levenberg-Marquardt. In *Proceedings of the IEEE/CVF International Conference on Computer Vision (ICCV)*, 2025. [6](#), [7](#), [8](#)
- [17] Binbin Jiang, Rui Huang, Qingyi Zhao, and Yuxiang Zhang. Gaussian difference: Find any change instance in 3D scenes. In *ICASSP 2025-2025 IEEE International Conference on Acoustics, Speech and Signal Processing (ICASSP)*, pages 1–5. IEEE, 2025. [1](#), [2](#)
- [18] Shyam Sundar Kannan and Byung-Cheol Min. ZeroSCD: Zero-shot street scene change detection. In *2025 IEEE International Conference on Robotics and Automation (ICRA)*, pages 4665–4671, 2025. [2](#)
- [19] Bernhard Kerbl, Georgios Kopanas, Thomas Leimkühler, and George Drettakis. 3D Gaussian splatting for real-time radiance field rendering. *ACM Trans. Graph.*, 42(4):139–1, 2023. [1](#), [2](#), [3](#), [4](#), [5](#), [6](#), [7](#), [8](#)
- [20] Jae-Woo Kim and Ue-Hwan Kim. Towards generalizable scene change detection. In *Proceedings of the Computer Vision and Pattern Recognition Conference*, pages 24463–24473, 2025. [1](#), [2](#), [5](#), [6](#)
- [21] Alexander Kirillov, Eric Mintun, Nikhila Ravi, Hanzi Mao, Chloe Rolland, Laura Gustafson, Tete Xiao, Spencer Whitehead, Alexander C Berg, Wan-Yen Lo, et al. Segment anything. In *Proceedings of the IEEE/CVF international conference on computer vision*, pages 4015–4026, 2023. [2](#)
- [22] Mathis Kruse, Marco Rudolph, Dominik Woivode, and Bodo Rosenhahn. Splatpose & detect: Pose-agnostic 3D anomaly detection. In *Proceedings of the IEEE/CVF Conference on Computer Vision and Pattern Recognition*, pages 3950–3960, 2024. [1](#), [2](#), [5](#), [6](#)
- [23] Mathieu Labb   and Fran  ois Michaud. RTAB-Map as an open-source lidar and visual simultaneous localization and mapping library for large-scale and long-term online operation. *Journal of field robotics*, 36(2):416–446, 2019. [3](#)

- [24] Seonhoon Lee and Jong-Hwan Kim. Semi-supervised scene change detection by distillation from feature-metric alignment. 2024 ieee. In *CVF Winter Conference on Applications of Computer Vision (WACV)*, pages 1215–1224, 2024. 2
- [25] Jinjie Lei, Duo Peng, Pingping Zhang, QiuHong Ke, and Haifeng Li. Hierarchical paired channel fusion network for street scene change detection. *IEEE Transactions on Image Processing*, 30:55–67, 2020. 2
- [26] Vincent Lepetit, Francesc Moreno-Noguer, and Pascal Fua. EPnP: An accurate O(n) solution to the PnP problem. *International Journal of Computer Vision*, 81(2):155–166, 2009. 4
- [27] Chun-Jung Lin, Sourav Garg, Tat-Jun Chin, and Feras Dayoub. Robust scene change detection using visual foundation models and cross-attention mechanisms. In *2025 IEEE International Conference on Robotics and Automation (ICRA)*, pages 8337–8343. IEEE, 2025. 2, 5, 6
- [28] Chin-Yang Lin, Cheng Sun, Fu-En Yang, Min-Hung Chen, Yen-Yu Lin, and Yu-Lun Liu. LongSplat: Robust unposed 3D Gaussian splatting for casual long videos. In *Proceedings of the IEEE/CVF International Conference on Computer Vision (ICCV)*, 2025. 3
- [29] Yizhe Liu, Yan Song Hu, Yuhao Chen, and John Zelek. SplatPose+: Real-time image-based pose-agnostic 3D anomaly detection. In *European Conference on Computer Vision Workshops*, pages 378–391. Springer, 2024. 1, 2, 3, 5, 6
- [30] Ziqi Lu, Jianbo Ye, and John Leonard. 3DGS-CD: 3D Gaussian splatting-based change detection for physical object rearrangement. *IEEE Robotics and Automation Letters*, 2025. 1, 2, 5, 6
- [31] Andreas Meuleman, Ishaan Shah, Alexandre Lanvin, Bernhard Kerbl, and George Drettakis. On-the-fly reconstruction for large-scale novel view synthesis from unposed images. *ACM Transactions on Graphics (TOG)*, 44(4):1–14, 2025. 3, 4
- [32] Ben Mildenhall, Pratul P Srinivasan, Matthew Tancik, Jonathan T Barron, Ravi Ramamoorthi, and Ren Ng. NeRF: Representing scenes as neural radiance fields for view synthesis. *Communications of the ACM*, 65(1):99–106, 2021. 1, 3
- [33] Maxime Oquab, Timothée Darcet, Théo Moutakanni, Huy Vo, Marc Szafraniec, Vasil Khalidov, Pierre Fernandez, Daniel Haziza, Francisco Massa, Alaeldin El-Nouby, et al. DINOV2: Learning robust visual features without supervision. *arXiv preprint arXiv:2304.07193*, 2023. 2
- [34] Jin-Man Park, Jae-Hyuk Jang, Sahng-Min Yoo, Sun-Kyung Lee, Ue-Hwan Kim, and Jong-Hwan Kim. ChangeSim: Towards end-to-end online scene change detection in industrial indoor environments. In *2021 IEEE/RSJ International Conference on Intelligent Robots and Systems (IROS)*, pages 8578–8585. IEEE, 2021. 1, 3, 5, 6
- [35] Guilherme Potje, Felipe Cadar, André Araujo, Renato Martins, and Erickson R Nascimento. Xfeat: Accelerated features for lightweight image matching. In *Proceedings of the IEEE/CVF Conference on Computer Vision and Pattern Recognition*, pages 2682–2691, 2024. 3
- [36] Jingxing Qian, Veronica Chatrath, James Servos, Aaron Mavrinac, Wolfram Burgard, Steven L Waslander, and Angela P Schoellig. Pov-slam: probabilistic object-aware variational slam in semi-static environments. *arXiv preprint arXiv:2307.00488*, 2023. 3
- [37] Nikhila Ravi, Valentin Gabeur, Yuan-Ting Hu, Ronghang Hu, Chaitanya Ryali, Tengyu Ma, Haitham Khedr, Roman Rädele, Chloe Rolland, Laura Gustafson, et al. SAM 2: Segment anything in images and videos. *arXiv preprint arXiv:2408.00714*, 2024. 4
- [38] Ragav Sachdeva and Andrew Zisserman. The change you want to see. In *Proceedings of the IEEE/CVF Winter Conference on Applications of Computer Vision*, pages 3993–4002, 2023. 1, 2, 5, 6
- [39] Ragav Sachdeva and Andrew Zisserman. The change you want to see (now in 3D). In *Proceedings of the IEEE/CVF International Conference on Computer Vision Workshops*, pages 2060–2069, 2023. 2
- [40] Ken Sakurada and Takayuki Okatani. Change detection from a street image pair using CNN features and superpixel segmentation. In *Proceedings of the British Machine Vision Conference 2015*, pages 61.1–61.12, Swansea, 2015. British Machine Vision Association. 1, 2
- [41] Ken Sakurada, Mikiya Shibuya, and Weimin Wang. Weakly supervised silhouette-based semantic scene change detection. In *2020 IEEE International conference on robotics and automation (ICRA)*, pages 6861–6867. IEEE, 2020. 2, 6
- [42] Paul-Edouard Sarlin, Cesar Cadena, Roland Siegwart, and Marcin Dymczyk. From coarse to fine: Robust hierarchical localization at large scale. In *Proceedings of the IEEE/CVF conference on computer vision and pattern recognition*, pages 12716–12725, 2019. 3
- [43] Lukas Schmid, Jeffrey Delmerico, Johannes L Schönberger, Juan Nieto, Marc Pollefeys, Roland Siegwart, and Cesar Cadena. Panoptic multi-tsdfs: a flexible representation for online multi-resolution volumetric mapping and long-term dynamic scene consistency. In *2022 International Conference on Robotics and Automation (ICRA)*, pages 8018–8024. IEEE, 2022. 3
- [44] Lukas Schmid, Marcus Abate, Yun Chang, and Luca Carlone. Khronos: A unified approach for spatio-temporal metric-semantic slam in dynamic environments. In *Proc. of Robotics: Science and Systems*, 2024. 3
- [45] Johannes L Schonberger and Jan-Michael Frahm. Structure-from-motion revisited. In *Proceedings of the IEEE conference on computer vision and pattern recognition*, pages 4104–4113, 2016. 2, 3
- [46] Aparna Taneja, Luca Ballan, and Marc Pollefeys. Image based detection of geometric changes in urban environments. In *2011 international conference on computer vision*, pages 2336–2343. IEEE, 2011. 1
- [47] Ashley Varghese, Jayavardhana Gubbi, Akshaya Ramaswamy, and P Balamuralidhar. ChangeNet: A deep learning architecture for visual change detection. In *Proceedings of the European conference on computer vision (ECCV) workshops*, pages 0–0, 2018. 2
- [48] Guanjun Wu, Taoran Yi, Jiemin Fang, Lingxi Xie, Xiaopeng Zhang, Wei Wei, Wenyu Liu, Qi Tian, and Xinggang Wang.

- 4D Gaussian splatting for real-time dynamic scene rendering. In *Proceedings of the IEEE/CVF conference on computer vision and pattern recognition*, pages 20310–20320, 2024. 2
- [49] Xiuzhe Wu, Peng Dai, Weipeng Deng, Handi Chen, Yang Wu, Yan-Pei Cao, Ying Shan, and Xiaojuan Qi. CL-NeRF: Continual learning of neural radiance fields for evolving scene representation. *Advances in Neural Information Processing Systems*, 36:34426–34438, 2023. 3, 6
- [50] Vladimir Yugay, Thies Kersten, Luca Carlone, Theo Gevers, Martin R Oswald, and Lukas Schmid. Gaussian mapping for evolving scenes. *arXiv preprint arXiv:2506.06909*, 2025. 3
- [51] Lin Zeng, Boming Zhao, Jiarui Hu, Xujie Shen, Ziqiang Dang, Hujun Bao, and Zhaopeng Cui. GaussianUpdate: Continual 3D Gaussian splatting update for changing environments. In *Proceedings of the IEEE/CVF International Conference on Computer Vision (ICCV)*, 2025. 2, 3, 6
- [52] Qiang Zhou, Weize Li, Lihan Jiang, Guoliang Wang, Guyue Zhou, Shanghang Zhang, and Hao Zhao. PAD: A dataset and benchmark for pose-agnostic anomaly detection. *Advances in Neural Information Processing Systems*, 36:44558–44571, 2023. 1, 2, 5, 6
- [53] Liyuan Zhu, Shengyu Huang, Konrad Schindler, and Iro Armeni. Living scenes: Multi-object relocalization and reconstruction in changing 3d environments. In *Proceedings of the IEEE/CVF Conference on Computer Vision and Pattern Recognition*, pages 28014–28024, 2024. 3